Effects of TRMM Boost on Oceanic Rainfall Estimates Based on Microwave Emission Brightness Temperature Histograms (METH)

DONG-BIN SHIN

Department of Atmospheric Sciences, Yonsei University, Seoul, South Korea

LONG S. CHIU

Center for Earth Observing and Space Research, George Mason University, Fairfax, Virginia, and Institute of Space and Earth Information Science, Chinese University of Hong Kong, Hong Kong, China

(Manuscript received 16 November 2007, in final form 6 March 2008)

ABSTRACT

A physical–statistical algorithm for estimating space–time average oceanic rainfall has been applied to microwave measurements taken by the Special Sensor Microwave Imager (SSM/I) on board the Defense Meteorological Satellite Program (DMSP) satellites and the Tropical Rainfall Measuring Mission (TRMM) Microwave Imager (TMI) on board the TRMM satellite. The algorithm is based on Microwave Emission Brightness Temperature Histograms (METH) and produces monthly rainfall over 5° × 5° latitude–longitude boxes as a TRMM standard product (3A11). The TRMM satellite was boosted from an altitude of 350–402 km in August 2001 to extend its mission life. The orbit boost affected the orbital parameters, rain-rate–brightness temperature relations, and then rain-rate parameters. Using oceanic rain rates derived from SSM/I, the difference between 3A11 and SSM/I for the preboost and postboost periods was analyzed. The difference shows a significant jump from the preboost to the postboost data if no adjustments were made for the postboost TRMM data. The jumps in rain-rate parameters are attributed to the changes in earth's incidence angle of TMI, affecting the brightness temperature in the TMI channels, the retrieved altitude of the freezing level, and the beam-filling correction factor. The changes in the brightness temperature (and freezing level) estimates and the beam-filling correction factor accounted for differences of approximately 4.9% and 1.5%, respectively. After the orbital and radiometric parameters are corrected for the boost, there is no detectable jump between the pre- and postboost 3A11 rain rates. The intersatellite calibration results demonstrate the robustness of the technique in producing a long record of climate-scale oceanic rainfall.

1. Introduction

A physical–statistical algorithm based on the microwave emission brightness temperature histograms (METH) has been developed by Wilheit et al. (1991) to estimate monthly oceanic rainfall. The METH algorithm has been applied to microwave brightness temperature (T_B) data collected by the Special Sensor Microwave Imager (SSM/I) taken on board the Defense Meteorological Satellite Program (DMSP) satellites. The dataset (July 1987–present) serves as an input to the global rain maps produced by the Global Precipitation Climatology Project (GPCP) and is available from the GPCP Polar Satellite Precipitation Data Center (PSPDC; http://gpcp-pspdc.gmu.edu/).

The algorithm was modified and applied to the Tropical Rainfall Measuring Mission (TRMM) Microwave Imager (TMI) data to produce a TRMM level 3 standard product (3A11) of monthly oceanic rainfall over 5° × 5° latitude–longitude boxes. In August 2001, the TRMM satellite was boosted from its nominal altitude of 350 km to an altitude of 402 km. The boost extends the TRMM satellite life, possibly into the TRMM follow-on mission of the Global Precipitation Measurement Mission (GPM) era. The potential overlap of TRMM with GPM can provide calibrations between the two rainfall missions, thus creating a long time series of global rainfall for climate change studies.

Corresponding author address: Dong-Bin Shin, Department of Atmospheric Sciences, Yonsei University, Shinchan-dong, Seodaemun-gu, Seoul 120-749, South Korea.
E-mail: dbshin@yonsei.ac.kr

DOI: 10.1175/2008JTECHA1093.1

TABLE 1. Comparison of SSM/I *F13*, TMI preboost, and TMI postboost channels (GHz), earth incidence angles (EIA, degrees), and footprint sizes (# km × # km) characteristics.

	EIA	Footprint for different channels				
SSM/I–*F13*	53.1	—	19.4	22.2	37.0	85.5
			69 × 43	50 × 40	37 × 28	15 × 13
		10.7	19.4	21.3	37.0	85.5
TMI preboost	52.8	63 × 37	30 × 18	23 × 18	16 × 9	7 × 5
TMI postboost	53.4	72 × 43	35 × 21	26 × 21	18 × 10	8 × 6

After the boost, a number of parameters in the rain algorithm TMI 3A11 are changed. The higher altitude increases the TMI earth's incidence angle and path, thereby changing the brightness temperature in all channels. The footprint size is also increased, which affects the so-called beam-filling error. In this report, we examine the impact of the estimated monthly rain rate if no adjustment was made in the postboost TRMM parameters. The postboost parameters are then applied to the postboost data. To calibrate the change, SSM/I rain rates estimated using the METH technique, or simply denoted SSM/I rain rates computed from the DMSP *F13* satellite, is used as a baseline. *F13* has been in nominal operation in this period and hence provides a rather homogeneous record for comparison. By examining the difference between these two products, which are based on the same methodology but with different sensor data input, climate signals that act as noise in the change detection of the boost are effectively filtered out.

2. Sensors and data characteristics

The TRMM Microwave Imager measures upwelling microwave radiances (brightness temperatures) emitted by the earth and atmosphere at five frequencies, 10.7, 19.4, 21.3, 37.0, and 85.5 GHz, with both horizontal and vertical polarizations (only vertical polarization at 21.3 GHz). At an altitude of 350 km, the radiometer views the atmosphere at an oblique angle (49°) corresponding to an earth incidence angle of 52.8°. The swath width of the TMI is 758.5 km. At each frequency the fields of view (FOVs) are determined by the satellite altitude, antenna size, and beamwidth. The effective FOV at 10.7 GHz is 63 km by 37 km (downtrack and crosstrack direction). The SSM/I is a seven-channel, four-frequency (19.35, 22.235, 37, and 85.5 GHz) microwave radiometer onboard the DMSP satellites in a sun-synchronous orbit. The details on SSM/I can be found in Hollinger et al. (1990). The DMSP satellites are sun synchronous while TRMM is non–sun synchronous. Table 1 shows the channel and orbit parameters of the SSM/I and of the TMI preboost and postboost configurations.

The METH (Wilheit et al. 1991) technique is based on a brightness temperature–rain-rate (R) relation (T_B–R) derived from the radiative transfer calculation of a cloud model. The cloud model uses a Marshall–Palmer distribution of raindrops (Marshall and Palmer 1948) from the ocean surface to the freezing level (FL, 0°C isotherm). A layer of cloud containing 0.5 g m^{-3} water content is assumed in the layer 0.5 km immediately below the FL. A constant lapse rate of 6.5°C km^{-1} and a relative humidity that increases linearly with height from 80% at the ocean surface to 100% at the freezing level are assumed. A combination channel of twice the 19.4-GHz minus the 21.3-GHz vertical polarization value for TMI, to mitigate the effect of water vapor (WV), is used for the T_B. The T_B over a space–time box is accumulated and the histogram computed. The computed T_B histograms are fitted iteratively to a rain-rate distribution via the T_B–R relation. The rain rate distribution is assumed to be mixed-lognormal. Since the humidity and temperature profiles are specified, the freezing level is a proxy of the columnar humidity content. The T_B responds to the integrated effect of precipitation drops over the rain column. Errors in the FL will then impact the rain rate in a negative sense (Chiu and Chang 2000). The altitude of the freezing level is determined using information from the upper 99th percentile of the 19.4- and 21.3-GHz brightness temperature histograms. To correct the beam-filling error, a freezing-height dependent, beam-filling correction (BFC) factor based on modeling and empirical results of Wang (1995) and Chiu et al. (1990) is used.

In the estimation procedure, the input parameters are the monthly brightness temperature histograms and their moments at every 5° latitude by 5° longitude box, and the mean brightness temperature of the upper 99th percentile at 19 and 22 GHz. The output parameters are FL; T_0 and σ_0, which are the mean and standard deviation (SD) of the nonraining part of the T_B histogram; and p, the fractional rain rate and the mean and SD of the conditional rain rates. Also, T_0 is used to adjust the T_B in the nonraining case.

The TRMM monthly oceanic rainfall data (3A11 version 6) for the period between January 1998 and De-

cember 2005 are used. The corresponding SSM/I *F13* rainfall data based on the same METH algorithm is available from the GPCP Polar Satellite Precipitation Data Center Web site (http://gpcp-pspdc.gmu.edu).

3. Boost effects of 3A11

The effects of the orbit boost in 3A11 can be described by two factors. First, the orbit boost increases the FOV size, then the beam-filling correction. The beam-filling error arises because of the coupling of the inhomogeneity of rain rates within the FOV and a nonlinear T_B–R relationship. Chiu et al. (1990) computed the percent bias due to the BFC as a function of the FOV size (square root of the FOV area) $\beta = R_T - R_E/R_T$, where R_E and R_T are, respectively, the estimated and true rain rate within the FOV. The true rain rate is therefore $R_T = F_{\mathrm{BFC}}R_E$, where the beam-filling correction factor (F_{BFC}) is $1/(1 - \beta)$. Wang (1995) examined the beam-filling effect and proposed a dependence of the BFC on FL. Based on Chiu et al. (1990, their Fig. 5), β is approximately 0.37 for FOV of ~20 km [$\sqrt{(23 \times 18)}$] and 0.38 for FOV of ~23 km [$\sqrt{(26 \times 21)}$]. The F_{BFC} are 1.587 for preboost and 1.612 for postboost FOVs at 22 GHz. The increase in F_{BFC} is therefore (1.612 – 1.587)/1.587, or approximately 1.5%. This simple correction has been applied to version 6 of 3A11.

The change of the TRMM satellite altitude also increases the earth incidence angle. The change in incidence angle results in change in the microwave surface emissivity, which is generally a function of frequency, incidence angle, polarization, the surface temperature, salinity, and surface roughness over the ocean surface. To understand the change of the brightness temperature due to the incidence angle, Fig. 1 shows the upwelling microwave radiances, expressed in brightness temperatures as a function of the vertically integrated (columnar) water vapor with incidence angles of 52.8° for the TRMM preboost and 53.4° for the postboost conditions for the combination channel (T_B, which is twice the vertically polarized 19.4-GHz brightness temperature minus 21.3-GHz brightness temperature: $2T_{\mathrm{B19V}} - T_{\mathrm{B21V}}$). A plane-parallel Eddington radiative transfer model is used to compute brightness temperatures at both TMI channels for the Wilheit cloud model (Wilheit et al. 1991; Shin and Kummerow 2003). The two curves are similar; T_B increases with increasing WV because of increased emission along the path. The postboost T_B is higher than the preboost T_B, due to an increase of the earth incidence angle results in a higher brightness temperature because the algorithm uses the vertically polarized channels. The longer pathlength also contributes to a higher brightness temperature but to a lesser degree.

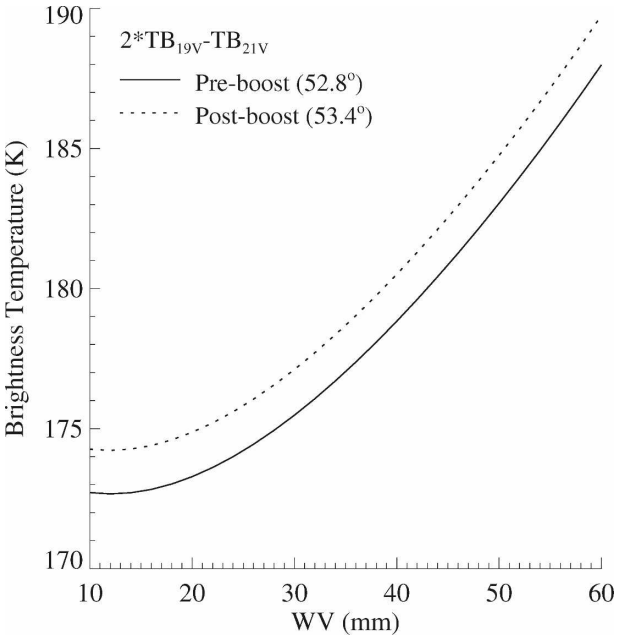

FIG. 1. Simulated brightness temperatures as a function of columnar WV with incidence angles of 52.8° for the TRMM preboost (solid line) and 53.4° for the postboost condition (dashed line). Brightness temperature is a linear combination of $2(T_{\mathrm{B19V}}) - T_{\mathrm{B21V}}$.

The freezing level is a proxy variable of the path-integrated water vapor. Figure 2 shows the time series of the difference between globally averaged FL estimated from SSM/I and that estimated in 3A11 (version 6). The global mean difference in the FL during the entire period is about 0.31 km. There is a distinct jump in the difference (TMI − SSM/I) between the preboost and postboost periods. A Student's t test shows significant difference at the 95% level of significance (Bulmer 1979).

We next examine the background brightness temperature T_0 in the algorithm; T_0 corresponds to the T_B in the absence of rain. Once the T_0 and FL are specified, the rain rates are determined by the T_B–R relation. The T_0 is therefore critical to selecting the appropriate T_B–R relations in the retrieval. Figure 3 illustrates the relationship between monthly-mean T_0 from TMI and that computed for SSM/I over the same 5° × 5° longitude–latitude grid boxes. The preboost and postboost periods, denoted by the pluses and diamonds, respectively, clearly show two distinct clusters. The regression lines of the two periods are also shown. The T_0 for the 3A11 and SSM/I are highly correlated (correlation > 0.99). The slopes of the regression lines are very similar (1.36 and 1.34), but the intercept is distinctly higher for the postboost period. The intercepts are −52.66 and −48.16 for the pre- and postboost periods, respectively.

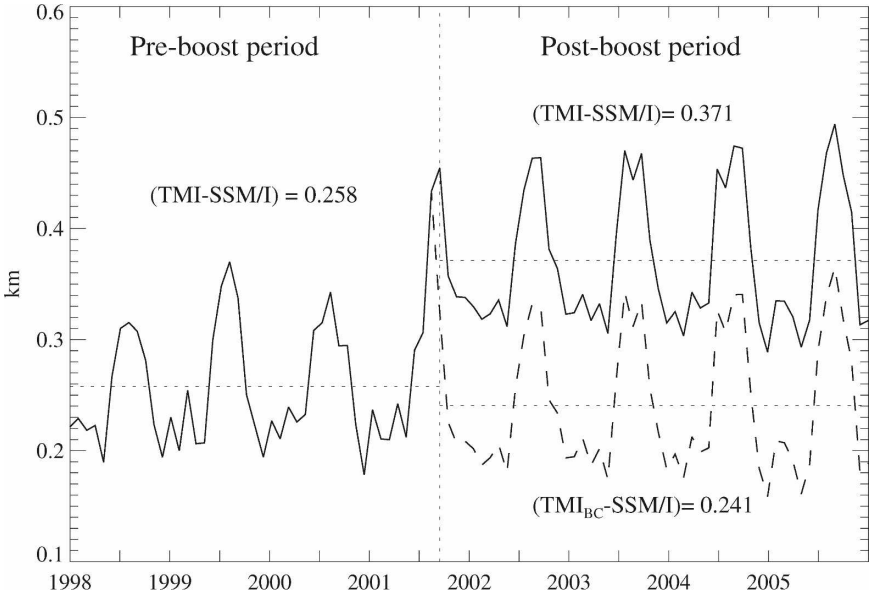

FIG. 2. Time series of the difference between TMI and SSM/I FL averaged over 40°S–40°N (solid line) from 1998 to 2006. The vertical dotted line shows the time of the TRMM boost in August 2001. The TMI FL with the boost effect correction (TMI_{BC}), which is discussed in section 4, is also compared with the SSM/I FL (dashed line) starting in August 2001.

4. Results with the adjustments

To account for the changes in the postboost orbital parameters, the monthly rainfall retrievals were performed with the following adjustments. The adjustments include the beam-filling correction, T_0 correction, and that for the combined case. The correction of T_0 is based on the result of Fig. 3. This simply involves subtracting the increased T_B (1.67 K) from the T_0 for the postboost period. These retrievals are also compared with the rainfall retrieved from SSM/I that are based on the same METH algorithm.

The upper panel of Fig. 4 shows the time series of monthly global mean rain rates from SSM/I and TMI retrievals without (TMI) and with (TMI_{BC}) correction for the orbit boost effects. The postboost correction (BC) contains both the beam-filling correction and T_0 correction (indicated by TMI_{BC} and dashed line). The SSM/I rain rates tend to show higher global rain rates than the other algorithms. The postboost corrections produce higher rain rates than those without the corrections. To focus on the pre- and postboost differences, the lower panel of Fig. 4 shows the time series of the TMI minus SSM/I rain rates (solid line). Their differences show a distinct jump at the TRMM boost (-0.223 mm day^{-1} for the preboost period versus -0.408^{-1} for the postboost period). However, after the corrections the difference between TMI_{BC} and SSM/I rainfall (dashed line) is reduced to -0.233 mm day^{-1},

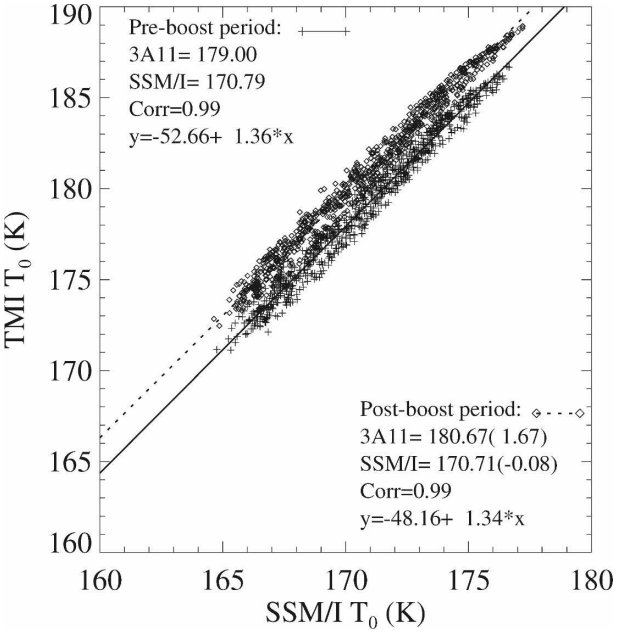

FIG. 3. Scatter diagrams of the background brightness temperature T_0 (monthly mean over 5° × 5° grid boxes) derived from TMI and SSM/I. The monthly background brightness temperature pairs from TMI (3A11) and SSM/I are indicated by the pluses and diamonds for the pre- and postboost periods, respectively. The regression lines are indicated by the solid and dotted lines for the two periods.

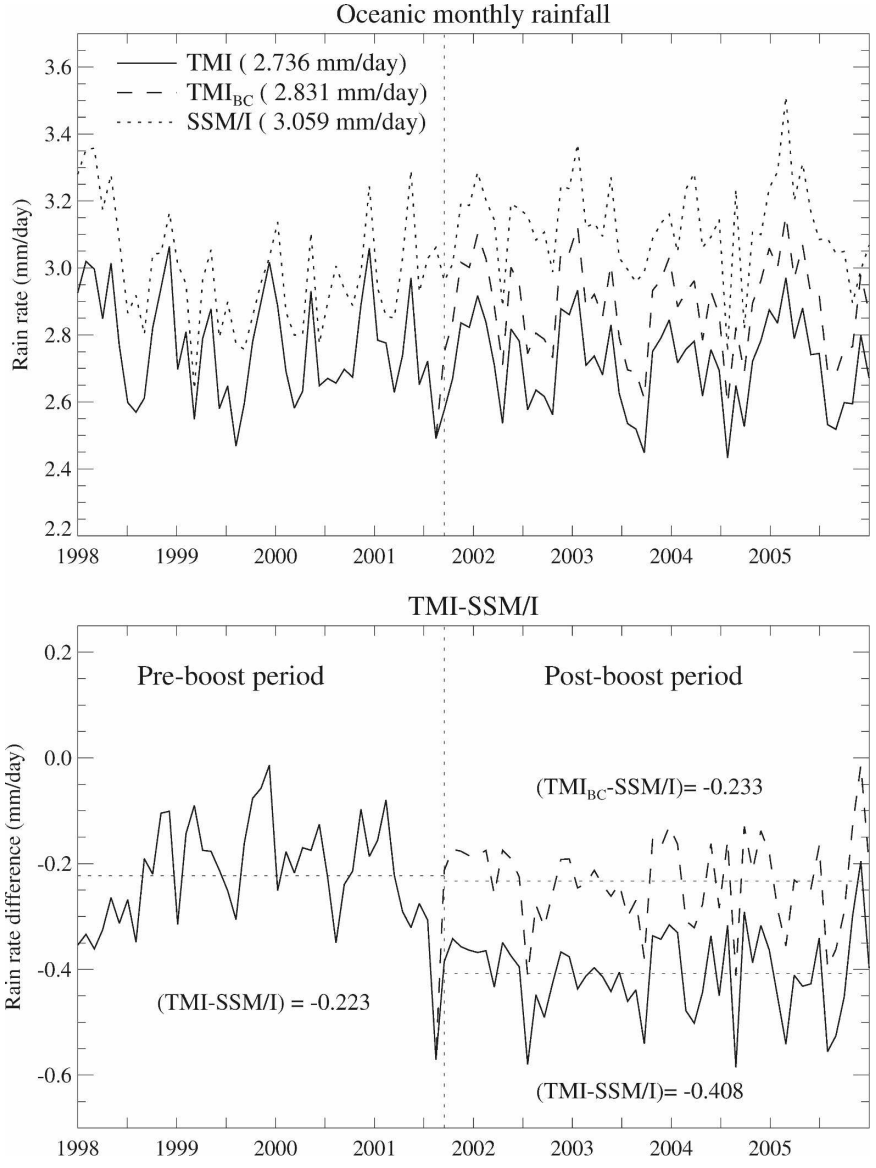

FIG. 4. (top) Monthly mean rainfall over ocean (40°S–40°N) for SSM/I (dotted) and TMI (3A11) with only BFC correction (TMI; solid line) and TMI with both BFC and T_0 corrections (TMI$_{BC}$; dashed line). The vertical dotted line shows the time of the TRMM boost in August 2001. (bottom) The differences between TMI rainfall and SSM/I rainfall for the pre- and postboost period.

which is not statistically different from the preboost difference (-0.223 mm day^{-1}) by a Student's t test at the 95% significance level.

The results of the corrections are summarized in Table 2. The first column indicates the correction types that include the BFC only, T_0 only, and BFC + T_0 corrections. It shows that the correction with the BFC only contributes to an increase of about 1.5% of 3A11 rain rates. The T_0 correction accounts for approximately 4.9%. The combined effect contributes to an

TABLE 2. Global mean rainfall from 3A11 algorithm with the specific correction types for the postboost period. The differences are obtained by subtracting the TMI rainfall without any corrections from the TMI rainfall with the specific corrections.

Correction type	Global average (mm day^{-1})	Difference (mm day^{-1})	Difference in percent
None	2.712	—	—
BFC only	2.753	0.041	1.5%
T_0 only	2.845	0.133	4.9%
BFC + T_0	2.887	0.175	6.5%

increase of the noncorrected rainfall by 6.5%. With these corrections, there is no distinct jump between the preboost and postboost 3A11 rain rates.

5. Summary and conclusions

The boost of the TRMM satellite to a higher orbit in August 2001 prolongs the satellite's life and allows continuing measurements of tropical precipitation systems since the launch of the satellite in 1997. This orbit boost changed the characteristics of the sensors as well as the orbital characteristics. In particular, rainfall estimations from TMI are affected by changes in the satellite altitude and then the increased incidence angle of TMI from 52.8° to 53.4°, resulting in decreasing the resolutions of the TMI's channel and changes in radiometric signatures primarily associated with surface emissivity.

This study examines the effect of changes in T_0 and BFC of the orbit boost on the TRMM 3A11 algorithm. To focus on the changes between the preboost and postboost period, the SSM/I rain rates estimated from the DMSP *F13* satellite using a similar technique are used for calibrating the differences. It is found that the microwave brightness temperatures response to water vapor is greater for the preboost than for the postboost configurations because of the increased incidence angle. The freezing level (FL) is a proxy variable to be determined in most microwave retrieval algorithms. The FL from TMI 3A11 is compared to the SSM/I-driven FL. The TMI 3A11 appears to estimate higher FL by 0.129 km during the postboost period than the preboost period. Since the estimation of FL is closely related to the determination of the background brightness temperature T_0 in the algorithm, T_0 has been compared for the pre- and postboost periods; T_0 is found to be higher for the postboost period than the preboost period. The increase in T_0 due to the orbit boost is about 1.67 K in the absence of rain and the difference decreases for higher water vapor content.

An effort has been made to investigate the effects of the orbit boost on the 3A11 algorithm by applying the individual adjustments to the algorithm. The individual adjustments include the beam-filling effect and T_0 correction and the combined case. The results showed that the difference in monthly rainfall for the pre- and postboost period can be reconciled by taking into account the beam-filling and T_0 corrections. It is also shown that the effect due to changes in T_0 has a greater impact on the 3A11 rain rates than the beam-filling correction.

DeMoss and Bowman (2007) compare the biases of the TRMM level 2 rain-rate algorithms [TMI 2A12 and Precipitation Radar (PR 2A25)] with the National Oceanic and Atmospheric Administration (NOAA) buoy gauges over the tropical oceans. They found a significant difference of >10% (0.4 mm day^{-1}) for TMI 2A12 and about 7% (which was judged to be insignificant) of the PR 2A25 rain rates over the buoy gauges. From our analysis, the global bias between the preboost and postboost 3A11 rain rates is 0.17 mm day^{-1} or 6.5%, which is judged to be significant using a Student's t test.

Finally, the strength of the METH method is its robustness and self-calibration. Once the T_0 and FL are determined, they specify completely the T_B–R relation. In this paper, we use rain-rate parameters estimated from the SSM/I *F13* data as a basis for comparison to focus on the changes before and after the boost. With the BFC and T_0 corrections, they account for most of the differences between the preboost and postboost 3A11 rain rates. The implication is that this technique is capable of producing climate-scale global oceanic rain rates for climate trend studies using multiple overlapping satellite sensors.

Acknowledgments. We thank Drs. Robert Adler and Tom Wilheit for suggestions and comments. DBS also thanks Dr. Jung Moon Yoo for his comments and encouragement. The TRMM data are processed by the TRMM Science and Data Information System and distributed by the NASA GSFC Distributed Active Archive Center. This work is supported by the NASA TRMM program. DBS was supported by the Korea Foundation for International Cooperation of Science & Technology (KICOS) through a grant provided by the Korean Ministry of Science & Technology (MOST) (K20701010357-07B0100-10710).

REFERENCES

Bulmer, M. G., 1979: *Principles of Statistics*. Dover, 252 pp.

Chiu, L. S., and A. T. C. Chang, 2000: Oceanic rain column height derived from SSM/I. *J. Climate,* **13,** 4125–4136.

——, G. R. North, D. A. Short, and A. McConnell, 1990: Rain estimation from satellites: Effect of finite field of view. *J. Geophys. Res.,* **95,** 2177–2185.

DeMoss, J. D., and K. Bowman, 2007: Changes in TRMM rainfall due to the orbit boost estimated from buoy rain gauge data. *J. Atmos. Oceanic Technol.,* **24,** 1598–1607.

Hollinger, J. P., J. L. Peirce, and G. A. Poe, 1990: SSM/I instrument evaluation. *IEEE Trans. Geosci. Remote Sens.,* **28,** 781–790.

Marshall, J. S., and W. M. Palmer, 1948: The distribution of raindrops with size. *J. Meteor.,* **5,** 165–166.

Shin, D.-B., and C. Kummerow, 2003: Parametric rainfall retrieval algorithms for passive microwave radiometers. *J. Appl. Meteor.,* **42,** 1480–1496.

Wang, S. A., 1995: Modeling the beamfilling correction for microwave retrieval of oceanic rainfall. Ph.D. dissertation, Texas A&M University, 99 pp.

Wilheit, T. T., A. T. C. Chang, and L. S. Chiu, 1991: Retrieval of monthly rainfall indices from microwave radiometric measurement using probability distribution functions. *J. Atmos. Oceanic Technol.,* **8,** 118–136.